Alzheimer's & Dementia: Diagnosis, Assessment & Disease Monitoring 2 (2016) 39-48

Alzheimer's & Dementia

Diagnostic Assessment & Prognosis

Learning to classify neural activity from a mouse model of Alzheimer's disease amyloidosis versus controls

Shlomit Beker[a,*], Vered Kellner[a,‡], Gal Chechik[a], Edward A. Stern[a,b]

[a]*Gonda Brain Research Center, Bar-Ilan University, Ramat Gan, Israel*
[b]*MassGeneral Institute for Neurological Disease, Department of Neurology, Massachusetts General Hospital, Charlestown, MA, USA*

Abstract The mechanisms underlying Alzheimer's disease (AD) onset and progression are not yet elucidated. The extent to which alterations in the activity of individual neurons of an AD model are significant, and the phase at which they can be captured, point to the intensity of the pathology and imply the stage at which it can be detected. Using a machine-learning algorithm, we present a successful cell-by-cell classification of intracellularly recorded neurons from the B6C3 APPswe/PS1dE9 AD model, versus wildtypes controls, at both a late stage and at an early stage, when the plaque pathology and behavioral deficits are absent or rare. These results suggest that the deficits present in neuronal networks of both old and young transgenic animals are large enough to be apparent at the level of individual neurons, and that the pathology could be detected in nearly any given sample, even before pathologic signs.

Keywords: Alzheimer's disease; Amyloid-β; SVM; Classification; Machine-learning

1. Introduction

The resolution and the stage in which information on an Amyloid-β (Aβ)–related pathology can be detected in the brain are not well studied. An automated detection of neurons and neural assemblies that provides information about the pathology would be valuable for Alzheimer's disease (AD) research, and could assess the predictive power of various physiological features found in these mice, and constitute a set of parameters indicative of the pathology in the early stages.

Although the accumulation and aggregation of Aβ in the brain are postulated to be a central event in the pathogenesis of AD, different lines of evidence support the presence of a preclinical phase in the development of the disease, where Aβ abnormality begins before the onset of the clinical disease [1–4]. Other studies consider the soluble form of Aβ to be a major factor in cognitive decline [5,6]. Two crucial questions that could impact both the progress of the disease and early detection are whether any information about the pathology can be retrieved from individual neurons and whether this information is available in a pre-symptomatic stage.

It was recently shown that the coherence of neural activity in various cortical areas of the APP/PS1 transgenic (Tg^+) mice model *in vivo* is reduced compared to wildtype (WT) controls at different stages of AD [7–9]. It was proposed that this reduction in coherence of the network activity is linked to the malfunctioning of individual neurons. Recent evidence also showed a profound disruption of slow oscillations of cortical assemblies by pathological Aβ, that was elevated either chronically in the APP23 × PS45 mouse model, or acutely after exogenous administration [9]. Disruption to slow oscillations was also linked to tau pathology [10].

Although the aforementioned alterations were statistically evident at the group level, it is still not known how robust they are and whether they can be captured in individual cells at different stages of the pathological cascade. If a neuron-by-neuron classification based on physiological differences between APP/PS1 Tg^+ and WT mice is

‡Current affiliation: Max Planck Florida Institute, Jupiter, FL.
*Corresponding author. Tel.: +972-3-523281428; Fax: +972-3-5352184.
E-mail address: shlomitbeker@gmail.com

http://dx.doi.org/10.1016/j.dadm.2016.01.002

successful, it would imply that the effects are consistent across neurons, and that the detrimental effects of Aβ are evident in most neurons even before the appearance of significant plaque aggregation.

In this article, we describe how electrophysiological activity can be robustly classified when measured from APP/PS1 Tg^+ mice and littermate controls, using a support vector machine (SVM). Because they are data driven, automated algorithms for classification can be more accurate and more consistent than classification defined by human rules. Classification was applied on physiological features from three levels of cortical recordings *in vivo*: intracellular recordings, LFP (local field potentials), and ECoG (electrocorticogram). Although the LFP and the ECoG recordings reflect summation of electric activity over neuronal populations, intracellular recordings provide the physiological underpinnings of such activity. The physiological features used in this study pointed to reduced coherence and suggest an increased perturbation to neuronal activity. Recordings were obtained from animals from two age groups: young, before the emergence of significant Aβ plaque pathology and related behavioral deficits, and old, at an age when the cortex is burdened with Aβ plaques, and when various cognitive and behavioral impairments can be detected.

2. Methods

2.1. Data types

Data for classification were collected from recordings in the B6C3 APPswe/PS1dE9 transgenic mouse model (APP/PS1) and wildtype (WT) littermates. Supplementary Table 1 shows the ages of the animals used in all classifications. Classification results were obtained as elaborated below.

2.2. Data acquisition

Cortical activity was measured by three techniques: intracellular recordings, LFP, and ECoG.

2.2.1. Intracellular recordings

Each recording was made from an individual neuron from an APP/PS1 Tg^+ or WT mouse. Animals were from two age groups:

2.2.1.1. "Old" group: 9–19 months old

At this age, the cortex of the mouse model is burdened with Aβ plaques. We collected a total of $n = 19$ neurons: 13 WT, 6 Tg^+, from 12 and 6 animals, respectively.

2.2.1.2. "Young" group: 2–6 months old

This age range is before a significant onset of Aβ plaque pathology, whereas soluble Aβ is abundant in the cortex. We collected a total of $n = 26$ neurons: 15 WT (age: 3–6 months), 11 Tg^+ (age: 2–4 months) from 13 and 10 animals, respectively.

2.2.2. LFP of old group (9–19 months)

In this method, we recorded multicellular activity from a relatively small tissue volume in deeper layers of the cortex. A total of $n = 23$ recordings of LFP (12 WT, 11 Tg^+) were collected. After dura removal, LFP electrodes were inserted up to 300 μm below cortex surface.

2.2.3. ECoG recordings of the old group (9–19 months)

In this method, we recorded the multicellular activity of larger populations from superficial layers of the cortex. A total of $n = 23$ recordings of ECoG (12 WT, 11 Tg^+) were collected. ECoG electrodes were placed on top of the cortex above the dura.

LFP and ECoG were recorded in the same animals.

Fig. 1 shows examples of intracellular, LFP and ECoG recordings from APP/PS1 Tg^+ and WT, along with representative images of Aβ plaque pathology and cell staining from the two age groups.

2.3. Feature extraction and selection

We tested a series of features extracted from physiological parameters of recordings of APP/PS1 Tg^+ and WT mice in the two age groups. All the physiological features used by the classifiers are listed in Supplementary Table 2.

Each of the four classifiers used parameters from one dataset with one recording technique for the APP/PS1 Tg^+ and WT mice. These parameters captured different features of the recordings, and included the time-domain, and the frequency-domain from subthreshold or suprathreshold activity.

2.4. Classification setting

We trained a separate binary classifier on each of the data sets described in section 2.2 to solve the four classification "intracellular old", "intracellular young", "LFP", and "ECoG" problems. Each classification was done on the number of recordings (neurons/assemblies) in the respective dataset. The number of features used by each classifier is indicated in Supplementary Table 2.

The input for training each classifier was the set of electrophysiological features obtained for each of the examples (neurons/assemblies) in the respective dataset accompanied by a binary label indicating whether that example was a positive (Tg^+) or a negative sample (WT).

2.5. Classification algorithm

We used a linear SVM binary classifier [11]. Linear SVM is a supervised learning method which trains a hyperplane that maximizes the margin between the positive and negative samples. SVM inputs a set of labeled samples (x_i, y_i), where each sample is represented as a vector of input features $x_i \in R^d$, and is also labeled as positive (Tg^+) or negative (WT): $y_i \in \{+1, -1\}$.

SVM aims to solve the following optimization problem

$$\min_w \frac{1}{2}\|w\|^2 + C\sum_i \xi_i$$

$$\text{s.t. } y_i(w^T x_i + b) \geq 1 - \xi_i, \quad \xi_i \geq 0, \quad i = 1, \ldots, n$$

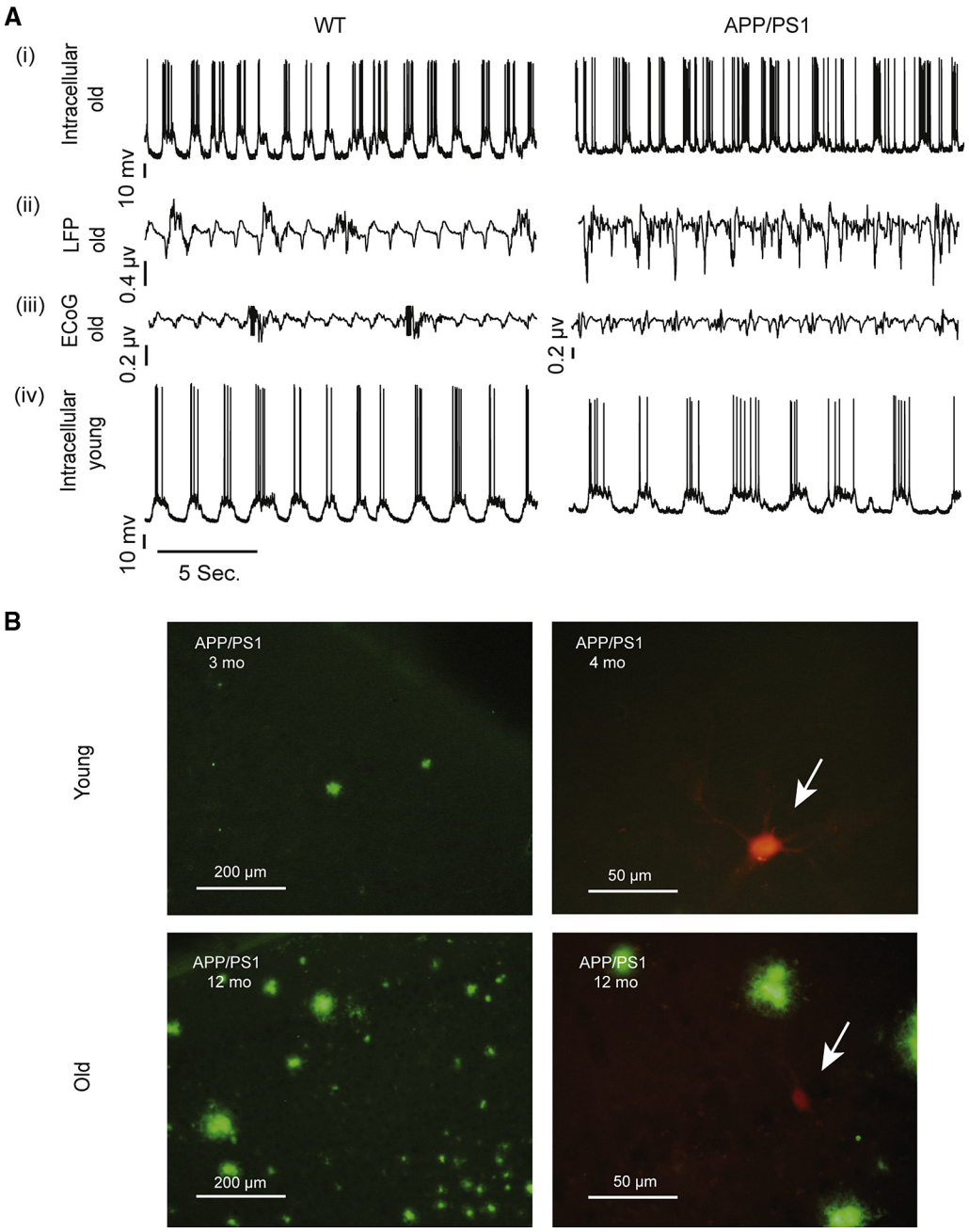

Fig. 1. Examples of recordings and immunostaining of neurons used in the classifications. (A) (i–iii) Intracellular, LFP, and ECoG recordings from old APP/PS1 Tg^+ animals, whose cortex is burdened with Aβ plaques (right) and WT controls (left). (iv) Recordings of intracellular activity of young mice, before a significant appearance of Aβ plaques (right), and their age-matched controls (left). (B) Thioflavin-S staining of Aβ plaques in APP/PS1 Tg^+ animals. Plaques are absent or rare in the cortex of young animals but abundant in the cortex of the old animals (bottom; left column figure magnification: x10; right column figure magnification: ×40). Recorded cells seen in red (marked by arrows) were filled with Alexa Flour 594 hydrozine for cell visualization. Abbreviations: LFP, local field potential; ECoG, electrocorticogram; Aβ, Amyloid-β.

To compensate for the unbalanced number of positive and negative samples in our data, we assigned different costs C^+ and C^- (instead of the uniform cost C in the above formulation) to false positive and false negative errors. Specifically, we tuned the value of a hyperparameter C over the grid {0.01, 0.1, 1, 10, 100} and set the value of C^+ to be C times the fraction of negatives, and C^- to C times the fraction of positive samples. We used the implementation of linear SVM available in Matlab R2011 b (MathWorks, Natick, MA).

2.6. Performance metrics

The linear classifier was trained for a binary decision problem predicting a Tg^+ versus WT recording. We assessed

performance using a leave-one-out procedure: the classifier was trained on all recordings (neurons/assemblies) except one. Then, we used the learned model to predict the class of the left-out sample. The procedure was repeated once for every recording (a total of 26 times for the young intracellular dataset, and 19 times for old intracellular dataset, and a total of 23 times for the LFP and ECoG data sets, separately), and the mean error is reported. This generated a contingency table with four categories: true positives (TP), i.e., recordings correctly labeled as taken from transgenic animals, false positives (FP), i.e., recordings incorrectly labeled as transgenic, true negatives (TN), i.e., recordings correctly labeled as nontransgenic, and false negatives (FN), i.e., recordings incorrectly labeled as nontransgenic. The accuracy of each classification was then evaluated using sensitivity and specificity. Sensitivity quantifies how well the classifiers correctly identify positive results (recordings from transgenic animals) and is defined as

$$\text{Sensitivity} = \frac{\text{TP}}{\text{TP}+\text{FN}}.$$

Specificity quantifies how well classifiers identify negative results (in our experiments, nontransgenic animals) and is defined as

$$\text{Specificity} = \frac{\text{TN}}{\text{TN}+\text{FP}}.$$

Overall accuracy is the proportion of sensitivity and specificity of all results, defined as:

$$\text{Accuracy} = \frac{\text{TN}+\text{TP}}{\text{TN}+\text{FP}+\text{FN}+\text{FP}}.$$

2.6.1. Receiver operator characteristic (ROC) curve

To evaluate the performance of each classifier, we plotted a receiver operator characteristic curve (ROC) [12]. The performance of the classifiers appears as a cumulative distribution function ranging from false positive (1 − specificity) to true positive (sensitivity) and uses the area under the curve (AUC) of each classification as the measurement of the overall quality of classification.

2.7. Bagging

To improve classification accuracy, we used bootstrap aggregation, also known as bagging [13], on all individual classifiers of the four data sets. Bagging combines the decisions of individual classifiers (voters) for every sample, to reach an agreement on classification of samples within each data set. For all data sets but ECoG, a positive vote was defined as 4 or more positive voters. Owing to the small number of features in the ECoG class, a positive vote was defined as $\geq$5 individual positive votes.

3. Results

3.1. Classification results

We tested four different types of recordings from APP/PS1 Tg^+ versus WT mice. To evaluate the classifiers, we computed their sensitivity, specificity, and overall accuracy, as well as the AUC. A summary of all the results, with the most predictive features, is presented in Table 1.

Hyper parameter C was chosen for each classification individually (see Supplementary Table 3 and Supplementary Fig. 1).

Overall, all four recording methods yielded high classification accuracies, achieving a mean sensitivity, specificity, and accuracy of 0.81, 0.75, and 0.78, respectively, across the four classifiers. Out of all the classifiers, intracellular old data achieved the highest sensitivity, specificity, and overall accuracy scores (0.83, 0.84, and 0.84, respectively). Performance metrics for classification of the four data sets are presented in Fig. 2A.

In terms of classification evaluation, classification of the intracellular old dataset was the most successful, with the highest yield (AUC = 0.95). followed by LFP, ECoG, and intracellular young (AUC = 0.84, 0.78, 0.69, respectively, and see Fig. 2B). The fact that the classifier of intracellular old recordings achieved the highest value implies that intracellular measurements of cells were the most characteristic of the AD pathology in our model.

Table 1
Summary of results for classifications of all data sets

Experiment	Intracellular old	LFP old	ECoG old	Intracellular young
Correct Tg^+	100 (6)	83.3 (11)	72.7 (11)	72.7 (11)
Correct WT	76.92 (13)	81.8 (12)	66.6 (12)	66.6 (15)
Overall	**84.2 (19)**	**82.6 (23)**	69.5 (23)	69.2 (26)
Overall after bagging	84.2 (19)	73.9 (23)	**82.6 (23)**	**76.9 (26)**
Hyper parameter C value	0.1	1	0.1	1
AUC of ROC	0.95	0.84	0.79	0.69
Most predictive features	• Failures	• R_2	• R_2	• Failures
	• ISI	• std trough amp.	• Integral δb	• CV Dwell time DS
	• Early-late Δ of firing rate	• Trough frequency	• Kurtosis	• Var. in firing rate within up-states

Abbreviations: LFP, local field potential; ECoG, electrocorticogram; WT, wildtype; Tg+, transgenic; AUC, area under the curve.

NOTE: Accuracy scores are in percentages (%). Number of cells (for intracellular recordings) or animals (for extracellular recordings) is in parentheses. In bold: reported scores.

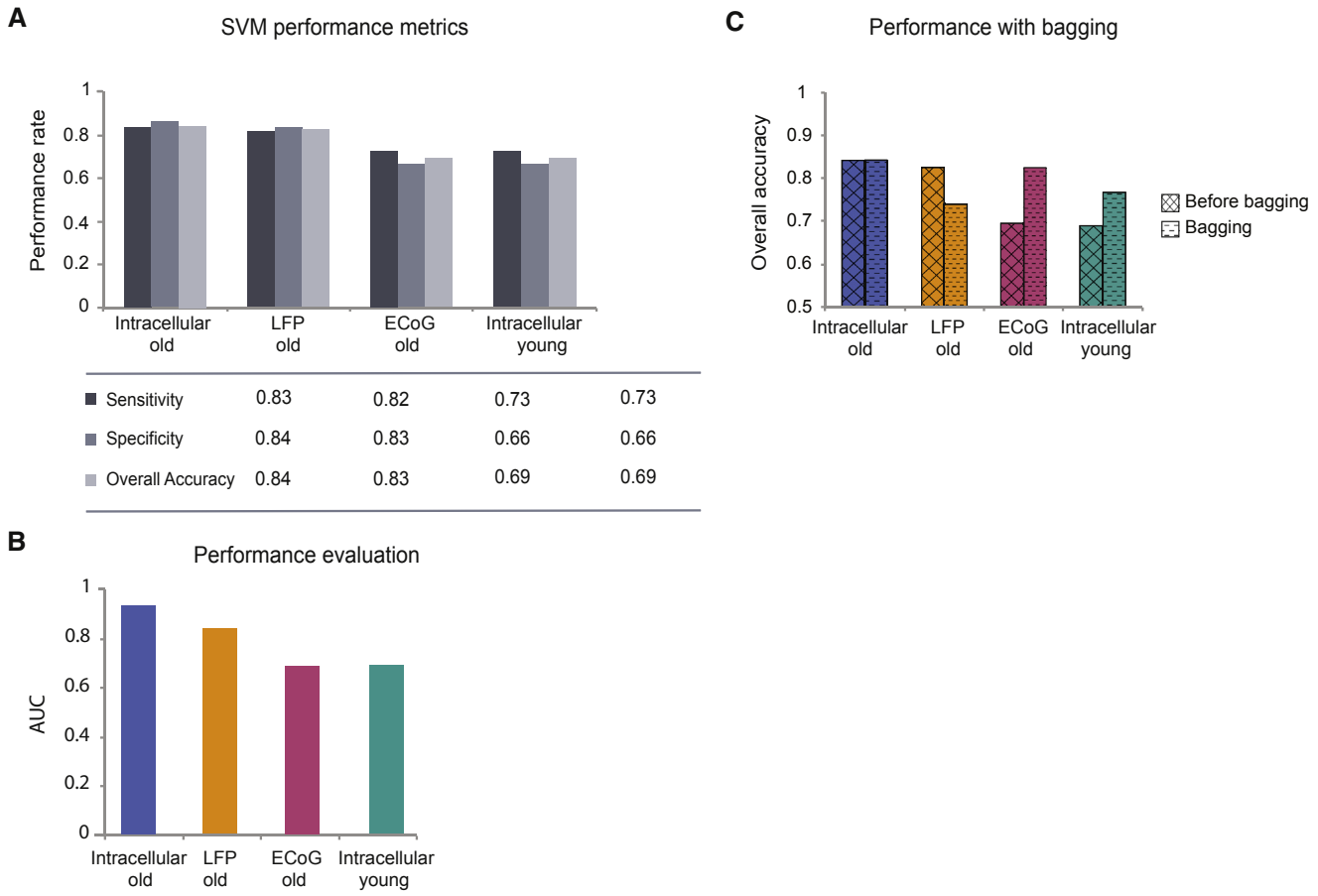

Fig. 2. Classification results. (A) Support vector machine performance metrics for the four classifiers. Sensitivity, specificity and overall accuracy which evaluated the precision of the classification predictions. (B) AUC (area under the curve) for the four classifiers. (C) Bagging voter results for all classifiers.

3.2. *The effect of bagging*

The current work operated in a regime where the number of samples was highly limited. In this regime, it is often hard to establish robustness with respect to the features used. To address this issue, we tested bagging [13]. Bagging operates by aggregating "votes" of classifiers trained on individual features, yielding a combined decision for each class. Fig. 2C shows prebagging and postbagging results.

Bagging votes improved the accuracy for the two classifiers with the lowest scores: ECoG (82.6%) and intracellular young (76.9%), as compared to the classifiers trained on all features (69.5% and 69.2%, respectively). It worsened, however, the accuracy of LFP classification (73.9%, comparing to 82% of all features classification) and did not have an effect on the intracellular old classification (84.2%).

3.3. *Individual feature classifiers*

To assess the efficiency of the four classifiers, we then looked more deeply into the predictive power of individual features in the four data sets. We trained single-feature classifiers (SFC) on each data set and compared them to combined feature classification (CFC). Fig. 3 shows the AUC measurements for classifiers that were trained on individual features (narrow bars), together with the AUC for classifiers trained jointly on all features of each dataset.

When comparing CFC and SFC, two effects were apparent: first, some of the CFCs had a seemingly lower performance than the best SFC for the same dataset. Second, some of the SFCs had an AUC <0.5, the performance level of random classification. Both are most likely a result of noisy evaluation due to the small number of samples. We next tested whether any of the CFCs came from a different distribution than the SFC. Although none of the SFCs were different from the CFC for each dataset in a statistically significant way, higher test statistics (and smaller P values) were obtained for the intracellular old (Wilcoxon $\rho = 9$, $P = .22$), and LFP (Wilcoxon $\rho = 11$, $P = .33$), compared to the ECoG (Wilcoxon $\rho = 5$, $P = .66$) and intracellular young (Wilcoxon $\rho = 6.5$, $P = .75$). In other words, the combined classifiers of the intracellular old and LFP had a performed better than the single-feature classifiers, relative to the two other data sets (ECoG and intracellular young).

When comparing the SFC of the different data sets across age groups, it is clear that some classifications shared some of the most predictive features. As shown in Fig. 3, both "Failures" and features related to firing rate ("Early-late Δ

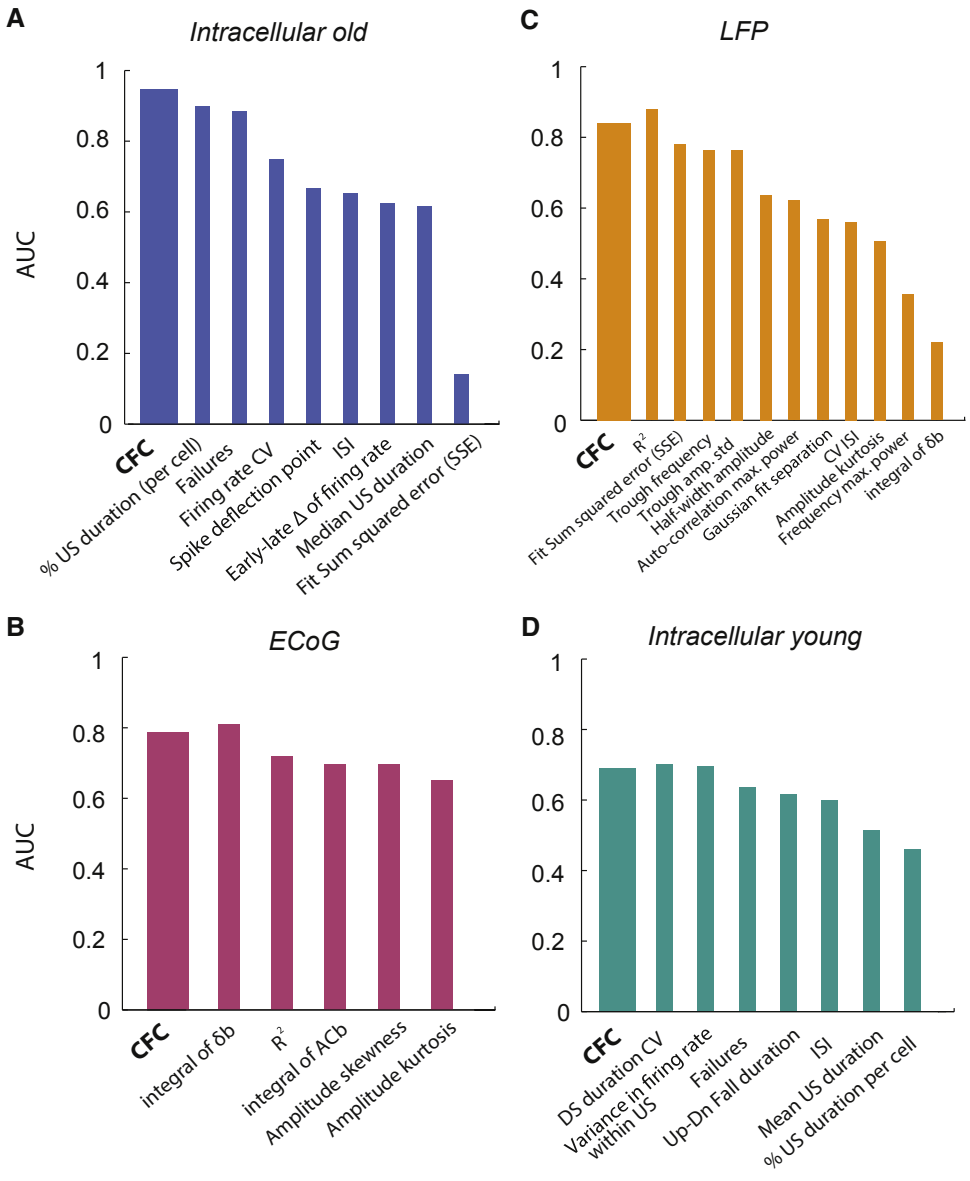

Fig. 3. Classification evaluation for individual features for the four datasets: (A) Intracellular old; (B) LFP; (C) ECoG; (D) Intracellular young. Wide bars represent area under curve (AUC) for combined feature classifiers (CFC). Narrow bars represent AUC for each of the single-feature classifiers (SFC).

of firing rate" in intracellular old; "Variance in firing rate within up states" in intracellular young) are among the best individual classifiers (see discussion).

3.4. Feature subset selection

To find the most predictive features and to eliminate redundant features in each classification, we used an L_1 regularization method, least absolute selection, and shrinkage operator (Lasso, [14]). The sparseness hyperparameter λ was chosen to eliminate all but the three most predictive features: intracellular old groups, $\lambda = 91$; LFP groups, $\lambda = 96$; ECoG groups, $\lambda = 88$; Intracellular young groups, $\lambda = 93$. Fig. 4 shows the most predictive features for the four classifiers.

4. Discussion

In this study, we successfully classified data from four types of cortical recordings from APP/PS1 AD transgenic mice and healthy controls, using a SVM. Although the vast majority of AD mouse models report the first cognitive deficits at 6 months of age at the earliest [15], we show that most cells of APP/PS1 Tg^+ mice can be automatically detected at 2–4 months of age, before any behavioral sign of the disease occurs, and before the pathological hallmarks appear in the brain.

This is, to the best of our knowledge, the first successful cell-by-cell classification of Tg^+ and WT neurons from an AD model. Importantly, we demonstrated a detection of the pathology during the early stage, when the pathology

has yet to appear. The fact that a high fraction of individual neurons can be correctly classified as pathological suggests that the pathophysiological properties that characterize this model are consistent across neurons and that AD progresses in a way where the pathology appears at the level of individual neurons, starting very early in the course of the disease.

Comparing the performance of the various classifiers that we trained provides insights into which characteristics are most informative about the disease (See 3.1). The highest accuracy (84%; area under the ROC curve [AUC] = 0.95) was achieved in classifying intracellular old recordings from individual cells of mice with substantial Aβ plaque deposition. A similar accuracy was achieved for LFP classification in the same age group (82%; AUC = 0.84). When using bagging, the overall success was improved for the other classifiers: ECoG (82.6%) and intracellular young (76.9%). Broadly speaking, with an exception of the classifier trained on intracellular young data, performance matched the spatial resolution of the recording involved. This coupling could be explained as follows: due to differences between neuronal populations in the cortex, variance of recordings increases along with the size of the neuronal population. Increased variance of features in the data set, in turn, might impact the performance of the classifier of this data set. Effects of

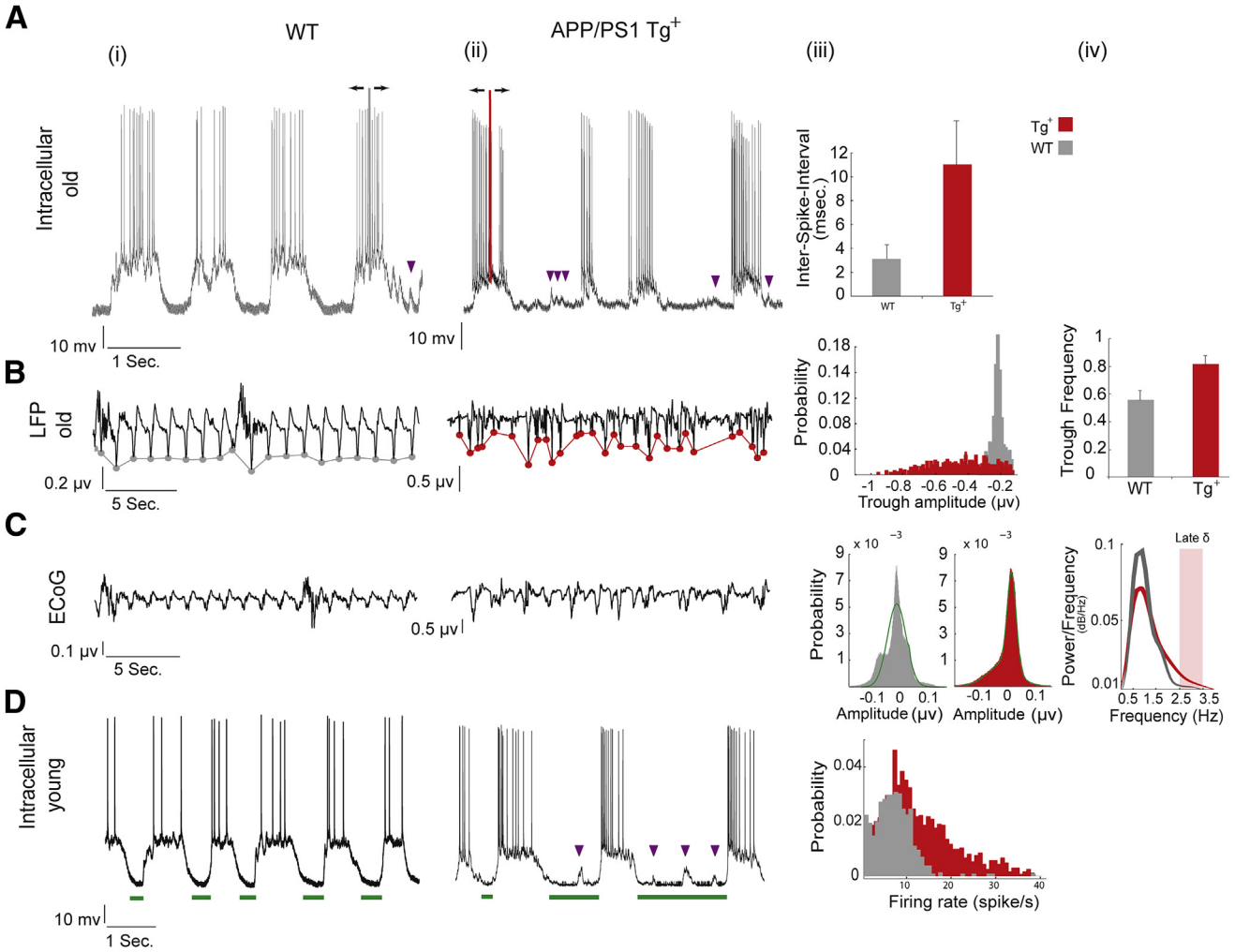

Fig. 4. Illustration of the most predictive features for classifying APP/PS1 Tg^+ recordings from wildtype (WT). (A) (i) WT intracellular recordings show fewer state-transition failures ("failures"; marked in purple arrowheads) than APP/PS1 Tg^+. (ii) In addition, recordings from APP/PS1 Tg^+ mice show stronger decay of firing rate over the up-state than the WT ("early-late Δ of firing rate"). Early and late segments of an up-state are marked by arrows and gray/red vertical lines in the middle of the WT/Tg^+ up-states, respectively. (iii) Bar graph that shows higher inter-spike-interval ('ISI') for APP/PS1 Tg^+ compared to WT cells. (B) (i) Examples of LFP recordings from WT and (ii) APP/PS1 Tg^+ mice. Recording of APP/PS1 Tg^+ shows higher variability of amplitude of troughs ("standard deviation of trough amp."), as well as higher trough frequency ("trough frequency"). (iii) Histogram for trough amplitudes, showing higher variability for APP/PS1 Tg^+, than WT. (C) Examples of ECoG recordings from (i) WT and (ii) APP/PS1 Tg^+ mice. (iii) A fit of Gaussians to the amplitude histogram ("R^2") was better for APP/PS1 Tg^+ ECoG recordings (red) than WT (gray). (iv) The power of the late delta band ("integral δb") is higher for APP/PS1 Tg^+ than WT. (D) Similar to the old APP/PS1 Tg^+ mice shown in (A), intracellular recordings of young APP/PS1 Tg^+ mice (purple arrowheads in (ii)) show more failures than WT (i). In addition, down-state duration (marked by green horizontal bars) increased in APP/PS1 Tg^+ neurons ("CV dwell time DS"). (iii) Variance in firing rate increased for APP/PS1 Tg^+ compared to WT cells, when measuring across up-states ("Variance in firing rate within up states").

reduced coherence in the APP/PS1 Tg^+ neuronal activity may act as an additional source of variability in the features recorded from larger neuronal networks, possibly accounting for the decreased classification accuracy in LFP and ECoG classifiers relative to intracellular young.

In addition to evaluating the performance of classifiers using combined feature classifiers (CFCs), we also evaluated single-feature classifiers (SFC). As expected, the AUC of CFCs was generally higher than that of SFCs for almost all data sets (Fig. 3), suggesting that the features used were synergistic and capture different predictive aspects of the data set, or that they allowed the classifiers to be more robust to noise. This means that despite the small number of samples, we generally controlled correctly for over fitting, and the classifiers operated in a regime where the feature dimensionality was appropriate. That said, a few individual features slightly surpassed the AUC of the CFC for LFP, ECoG, and intracellular young. This exception may be an artifact of the small number of samples and may disappear if larger data sets are used. The fact that the better classifiers (of intracellular old and LFP data sets) had a larger difference between their CFC and SFC, compared to the two others (ECoG, intracellular young), suggests that the combined classifiers of intracellular old and LFP better captured the dimensionality of the data.

Bootstrap aggregation (bagging) is an ensemble method where classifiers are trained on subsets of the data and then aggregated. Bagging can improve unstable learning procedures, with the risk of slightly degrading the performance of stable procedures [13]. Here we found that bagging improved the classification results for ECoG and intracellular young but did not change or even worsened results of the intracellular old and LFP data sets (see 3.2). As the procedure is based on votes for the most predictive individual features, cases that have lower performance of the CFC than the best SFCs improved more than ones with higher performance of the CFC than their SFCs.

Comparing the most predictive feature triplets (3.4 and Supplementary Table 2) provides insights into which physiological properties serve as the best predictors. The features with high predictive power were the following (respective data sets are in parenthesis):

1. "Failures" (intracellular old, intracellular young), refers to the fraction of uncompleted transitions from down-states to up-states in an intracellular voltage trace and was recently described in studies by our group on both the APP/PS1 Aβ model [8,9] as well as rTG4510, where tau is overexpressed [10]. Reduced neuronal activity caused by uncompleted transition to up-states leads to insufficient synchronized firing of action potentials and eventually to fragmentation of cortical networks into smaller networks, as signals fail to propagate to other parts of the network. Reduced coherence as seen in the recordings of LFP and ECoG [7] may lead to abnormal information processing. The high predictive power of this feature is further evidence of its robustness in the AD model.
2. "Fit R^2" (LFP, ECoG) captures how well the data can be fit with a bimodal distribution. While normally, the voltage distribution of neuronal activity is bimodal, reflecting the fluctuations between the silent and the active modes, voltage activity of APP/PS1 Tg^+ neurons display a weaker bimodality due to failures to up-state, and other perturbations to the regular state transitions. This reduced bimodality is a possible aspect of the pathology, and may have a greater impact on larger networks.
3. "Integral δb" (ECoG) which quantifies the power in the δ frequency band in the late part (2.5–3.5 Hz). This feature is of special importance as it is consistent with the slowing of the EEG found in AD patients, which was reflected in the high power in the low frequencies [2,4].

A body of research has pointed to electroencephalography (EEG) as a potential early indicative tool in AD patients [16,17]. Within that framework, characteristics such as perturbation to the synchrony of neuronal activity have been suggested as a way to differentiate AD from other forms of dementia. Based on these synchronization attributes, various methods for EEG classification and feature-selection have been reported to be good predictors of AD [18,19]. Nevertheless, there are several caveats to EEG as a diagnostic tool, in part due to its low signal-to-noise ratio. A direct measurement of neural activity from the mouse brain has a high signal-to-noise ratio and thus could advance and add reliability to current efforts to use noninvasive techniques for the detection of AD physiological markers among patients.

The features used by our classifiers support human scalp EEG studies by providing physiological correlates in a high spatial resolution to phenomena seen in the human EEG. Other features, such as "Fit R^2", could be modified and used as features in the classifications of EEG measurements from human AD patients versus controls.

The successful classification of the intracellular young dataset indicates the alterations in neuronal activity of APP/PS1 neurons are present at a stage when both the pathophysiology and the behavioral changes have yet to emerge. Although network disruptions and morphological changes are commonly associated with the late stage of the disease [20–22], the soluble form of Aβ, appearing at a pre-plaque phase of young mice, has also been linked to physiological changes, both *in vitro* [23–26], and *in vivo* [8], by affecting the intrinsic properties of neurons. Early detection of plaque-related pathology, even before cognitive and behavioral alterations occur in humans, could be an asset for AD research and treatment.

The present study relates to another frontier of AD research: the implementation of neural network models of AD. Several neural network models of AD have led to therapeutics suggestions, such as slowing down the degeneration

of synaptic connections [27], or strengthening of synaptic connections as compensation for the loss of others, at different stages of the disease [28]. Our results demonstrate the potential of inferring from a functional fallacy in one cell, through fallacies in larger networks, and eventually to the organism. This potential is applicable to computational models that predict the processes underlying the progression of the disease.

Acknowledgments

This work was supported by the National Institute on Aging at the National Institute of Aging (Grant Number AG024238), and the Legacy Heritage Bio-Medical Program of the Israel Science Foundation (Grant Number 688/10).

Supplementary data

Supplementary data related to this article can be found at http://dx.doi.org/10.1016/j.dadm.2016.01.002.

RESEARCH IN CONTEXT

1. Systematic review: The authors reviewed the literature using traditional (e.g., PubMed) sources. Most attempts to detect the Aβ pathology at early stages are focused on EEG measurements, and the emergence of the first cognitive changes. None of these studies has been able to detect the pathology before the pathophysiological or behavioral signs. No study has detected this pathology using data from a single neuron.
2. Interpretation: The fact that individual neurons of transgenic mice can be successfully detected, entails that the activity of single cells carries significant information about Aβ pathology, which is available before the onset of significant pathophysiological and behavioral changes.
3. Future direction: Our results highlight the dominance of the amyloid pathology in an early stage, which ultimately leads to neuronal degeneration and irreversible dementia. Novel features of the classification are proposed for AD research, to serve as early assessment, before the appearance of behavioral signs.

References

[1] Yau WY, Tudorascu DL, McDade EM, Ikonomovic S, James JA, Minhas D, et al. Longitudinal assessment of neuroimaging and clinical markers in autosomal dominant Alzheimer's disease: A prospective cohort study. Lancet Neurol 2015;14:804–13.

[2] Benzinger TL, Blazey T, Jack CR, Koeppe RA, Su Y, Xiong C, et al. Regional variability of imaging biomarkers in autosomal dominant Alzheimer's disease. Proc Natl Acad Sci U S A 2013; 110:E4502–9.

[3] Villemagne VL, Burnham S, Bourgeat P, Brown B, Ellis KA, Salvado O, et al. Amyloid β deposition, neurodegeneration, and cognitive decline in sporadic Alzheimer's disease: A prospective cohort study. Lancet Neurol 2013;12:357–67.

[4] Bateman RJ, Xiong C, Benzinger TLS, Fagan AM, Goate A, Fox NC, et al. Clinical and biomarker changes in dominantly inherited Alzheimer's disease. N Engl J Med 2012;367:795–804.

[5] Shankar GM, Li S, Mehta TH, Garcia-Munoz A, Shepardson NE, Smith I, et al. Amyloid-beta protein dimers isolated directly from Alzheimer's brains impair synaptic plasticity and memory. Nat Med 2008; 14:837–42.

[6] Lesné S, Koh MT, Kotilinek L, Kayed R, Glabe CG, Yang A, et al. A specific amyloid-beta protein assembly in the brain impairs memory. Nature 2006;440:352–7.

[7] Beker S, Goldin M, Menkes-Caspi N, Kellner V, Chechik G, Stern EA. Amyloid b disrupts ongoing spontaneous activity in sensory cortex. Brain Struct Funct 2014; [Epub ahead of print]. http://dx.doi.org/10.1007/s00429-014-0963-x.

[8] Kellner V, Menkes-Caspi N, Beker S, Stern EA. Amyloid-β alters ongoing neuronal activity and excitability in the frontal cortex. Neurobiol Aging 2014;35:1982–91.

[9] Busche MA, Kekuš M, Adelsberger H, Noda T, Förstl H, Nelken I, et al. Rescue of long-range circuit dysfunction in Alzheimer's disease models. Nat Neurosci 2015;18:1623–30.

[10] Menkes-Caspi N, Yamin HG, Kellner V, Spires-Jones TL, Cohen D, Stern EA. Pathological tau disrupts ongoing network activity. Neuron 2015;85:959–66.

[11] Vapnik V. The Nature of Statistical Learning Theory. New York: Springer-Verlag; 1995.

[12] Bradley AP. The use of the area under the ROC curve in the evaluation of machine learning algorithms. Pattern Recognit 1997;30:1145–59.

[13] Breiman L. Bagging predictors. Mach Learn 1996;24:123–40.

[14] Tibshirani R. Regression selection and shrinkage via the Lasso. J R Stat Soc B 1994;58:267–88.

[15] Webster SJ, Bachstetter AD, Nelson PT, Schmitt FA, Van Eldik LJ. Using mice to model Alzheimer's dementia: an overview of the clinical disease and the preclinical behavioral changes in 10 mouse models. Front Genet 2014;5:1–23.

[16] Jeong J. EEG dynamics in patients with Alzheimer's disease. Clin Neurophysiol 2004;115:1490–505.

[17] Uhlhaas PJ, Singer W. Neural synchrony in brain disorders: relevance for cognitive dysfunctions and pathophysiology. Neuron 2006; 52:155–68.

[18] Gallego-Jutglà E, Elgendi M, Vialatte F, Solé-Casals J, Cichocki A, Latchoumane C, et al. Diagnosis of Alzheimer's disease from EEG by means of synchrony measures in optimized frequency bands. Conf Proc IEEE Eng Med Biol Soc 2012;2012:4266–70.

[19] Gallego-Jutglà E, Solé-Casals J, Vialatte F, Elgendi M, Cichocki A, Dauwels J. A hybrid feature selection approach for the early diagnosis of Alzheimer's disease. J Neural Eng 2014;12:16018.

[20] Bero AW, Bauer AQ, Stewart FR, White BR, Cirrito JR, Raichle ME, et al. Bidirectional relationship between functional connectivity and amyloid- deposition in mouse brain. J Neurosci 2012;32:4334–40.

[21] Knowles RB, Wyart C, Buldyrev SV, Cruz L, Urbanc B, Hasselmo ME, et al. Plaque-induced neurite abnormalities: implications for disruption of neural networks in Alzheimer's disease. Proc Natl Acad Sci U S A 1999;96:5274–9.

[22] Spires TL, Meyer-Luehmann M, Stern EA, McLean PJ, Skoch J, Nguyen PT, et al. Dendritic spine abnormalities in amyloid precursor protein transgenic mice demonstrated by gene transfer and intravital multiphoton microscopy. J Neurosci 2005;25:7278–87.

[23] Busche MA, Eichhoff G, Adelsberger H, Abramowski D, Wiederhold K, Haass C, et al. Model of Alzheimer's Disease 2008.

[24] Rocher AB, Kinson MS, Luebke JI. Significant structural but not physiological changes in cortical neurons of 12-month-old Tg2576 mice. Neurobiol Dis 2008;32:309–18.

[25] Roder S, Danober L, Pozza MF, Lingenhoehl K, Wiederhold KH, Olpe HR. Electrophysiological studies on the hippocampus and prefrontal cortex assessing the effects of amyloidosis in amyloid precursor protein 23 transgenic mice. Neuroscience 2003;120: 705–20.

[26] Shemer I, Holmgren C, Min R, Fülöp L, Zilberter M, Sousa KM, et al. Non-fibrillar β-amyloid abates spike-timing-dependent synaptic potentiation at excitatory synapses in layer 2/3 of the neocortex by targeting postsynaptic AMPA receptors. Eur J Neurosci 2006;23:2035–47.

[27] Duch W. Computational models of dementia and neurological problems. Methods Mol Biol 2007;401:305–36.

[28] Ruppin E, Reggia JA. A neural model of memory impairment in diffuse cerebral atrophy. Br J Psychiatry 1995;166:19–28.